

Collaborative Position Control of Pantograph Robot using Particle Swarm Optimization

Nihad Ali, Yasar Ayaz, and Jamshed Iqbal*

Abstract: This article presents the design and real-time implementation of an optimal collaborative approach to obtain the desired trajectory tracking of two Degree of Freedom (DOF) pantograph end effector position. The proposed controller constructively synergizes the Proportional Integral Derivative (PID) and Linear Quadratic Regulator (LQR) by taking their weighted sum. Particle Swarm Optimization (PSO) algorithm is proposed to optimally tune the gains of PID, weighting matrices of LQR, and their ratio of contributions. Initially, the PID and LQR controller parameters are optimally tuned using PSO. In order to enhance the control effort and to provide more optimal performance, the weightages of each controller are optimally tuned and are kept constant. The collaborative position control strategy is tested against the PID and the LQR controllers via hardware in loop trials on a robotic manipulator. Experimental results are provided to validate the accurate trajectory tracking of the proposed controller. Results demonstrate that the optimal combination renders a significant improvement of 10% in steady-state response and about 37% in transient response over the PID and LQR schemes.

Keywords: Optimal control, pantograph, particle swarm optimization, robotics, rotary servo, tracking.

1. INTRODUCTION

Robotic manipulators are widely used in assembly lines for mounting, transporting, cutting, production, and welding, etc [1, 2]. Pantograph robotic manipulators are the most common types of robots used in industrial applications [3]. A pantograph is a mechanical linkage structure connected in a parallelogram-like manner. An accurate end effector's position of a manipulator is critical for high-performance robotic applications [4]. Control of a robotic manipulator deals with the problem of formulating the joint angles required to move an end-effector to follow a certain specified position trajectory. The kinematics of a manipulator and dynamics of actuators are derived to synthesize and physically realize the controller based on a certain hardware platform.

Precise position control of a robotic manipulator has received great attention of the researchers and engineers [5–8]. Most of these control algorithms are complex and do not provide generally an optimal performance. However, Linear Quadratic Regulator (LQR) and Proportional Integral Derivative (PID) controllers are still vastly used control strategies [9]. The LQR control law cannot com-

pensate modeling errors [10, 11]. In addition, the state and input weighting matrices define the control performance and must be adjusted optimally to achieve desired objectives. The tuning of a PID controller is practically intuitive. However, it does not guarantee the desired performance [12]. A properly tuned PID controller eradicates overshoot and steady-state error caused by transients in the response [13].

Tremendous research is being done to improve the position performance of robotic manipulators by combining PID and LQR controllers [14–16]. In [14], the gains of individual PID and LQR controllers are computed intuitively which is not an optimal way. Moreover, the combination of the gains of the two control laws is also non-optimal. Research work reported in [15] presents a FCPC scheme to control longitudinal dynamics of an aerial vehicle. However, the gains and weightage are not optimal. Similarly, in [16], the gains of PID and LQR controllers have not been optimized. However, fuzzy rules have been used to tune the weightages ξ_1 and ξ_2 of both the controllers. In contrast, we have used a single optimal weight h , thus reducing the optimization complexity. The perfor-

Manuscript received November 01, 2019; revised November 16, 2020 and February 8, 2021; accepted March 24, 2021. Recommended by Associate Editor Sehoon Oh under the direction of Editor Kyoung Kwan Ahn.

Nihad Ali is with Department of Robotics and Intelligent Machine Engineering, National University of Science and Technology, Islamabad, Pakistan and Department of Automation, Shanghai Jiao Tong University, Shanghai, China. (e-mail: nihad@sjtu.edu.cn). Yasar Ayaz is with the Department of Robotics and Intelligent Machine Engineering, National University of Science and Technology, Islamabad, Pakistan (e-mail: yasar@smme.nust.edu.pk). Jamshed Iqbal is with Department of Computer Science and Technology, Faculty of Science and Engineering, University of Hull, HU6 7RX, UK. (e-mail: j.iqbal@hull.ac.uk).

* Corresponding author.

mance cooperation can be further enhanced by optimizing the gains of the individual controller. Numerous optimization algorithms are reported in the literature. Metaheuristic Genetic Algorithm (GA) is used in many optimization problems [17–19]. The algorithm takes a very long time to search global best from a population of points rather than a single point [20]. Moreover, the conventional optimization tools intent to minimize the cost function only and do not contemplate some control objectives like reducing settling time, overshoot, and steady-state error [21]. In [19], the authors used two reactive evolutionary and four swarm-based algorithms including GA, differential evolution, Bat, hybrid Bat, cuckoo search, and Particle Swarm Optimization (PSO) to tune the PID control gains. Among these algorithm, PSO is the best candidate for optimization under the conditions of small population size and less iterations. The PSO method is addressed in the present research because of its ease in computation and quick convergence to the global minimum [22, 23]. Motivated by the abovementioned discussion, the main contributions of this paper are:

1) The PSO algorithm is used to optimally tune the design gains of PID and weighting matrices of LQR control schemes. In addition, their experimental validations are presented.

2) To overcome the disadvantages and to get the benefits offered by both control efforts, the weightage is optimally tuned via PSO to synthesize more efficient control algorithm. We design and implement a Fixed-weighted Collaborative Position Controller (FCPC) on a real-time 2-DOF pantograph robotic manipulator to improve its response in terms of settling time, steady-state error, and overshoot.

The remaining paper is organized in the following sections: Mathematical model of a 2-DOF robot manipulator is derived in Section 2. Section 3 presents the theoretical background of PID, LQR and the proposed FCPC control techniques. Parameter optimization is discussed in Section 4. The laboratory setup is described in Section 5. The experimental results and performance analysis of the proposed controller are presented in Section 6. Finally, concluding remarks are given in Section 7.

2. MATHEMATICAL MODEL

The present study considers a 2-DOF pantograph robot by Quanser, whose mathematical model is derived analytically. The robotic hardware benchmark consists of two identical rotary servo units (SRV02) connected together with a four-bar linkage [24]. The electrical circuit schematic including gears train of SRV02 is shown in Fig. 1. The load shaft position and speed dynamics for each SRV02 actuator are given by

$$\dot{\theta} = \omega \quad (1)$$

$$\dot{\omega} = -\frac{A}{R_m(J_m\eta_gk_g^2 + \tau_l)}\omega + \frac{\eta_mk_t}{R_m(J_m\eta_gk_g^2 + \tau_l)}v_m. \quad (2)$$

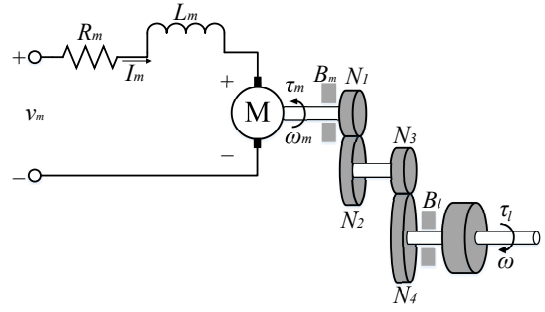


Fig. 1. SRV02 actuator schematic diagram.

where $A = R_m(B_m\eta_gk_g^2 + B_l) + \eta_mk_mk_t\eta_gk_g^2$. The electromechanical parameters used in this research and their nominal values are listed in Table 1, see [24, 25]. In [24], these parameters are experimentally verified using bump test and frequency response methods. In practical, these values may be slightly uncertain from the real robot. However, these uncertainties are not serious and brings only a small steady-state error [26], which we have ignored during the optimization process in section 4.

Table 1. Nomenclature

Parameter	Symbol	Value	Unit
actuator angular position	θ	–	rad
actuator angular velocity	ω	–	rad/sec
Rated voltage	V_g	6	V
Motor armature resistance	R_m	2.6	Ω
Total gear ratio	k_g	70	–
Motor back EMF constant	k_m	7.68×10^{-3}	Vsec/rad
Motor current-torque constant	k_t	7.68×10^{-3}	Nm
Gearbox efficiency	η_g	0.9	–
Motor efficiency	η_m	0.69	–
Rotor moment of inertia	J_m	3.9×10^{-7}	K_gm^2
Equivalent moment of inertia	J_{eq}	9.76×10^{-5}	K_gm^2
Equivalent damping coefficient	B_{eq}	0.015	Nmsec/rad
Length of bar linkage	L_b	0.127	m
Mass of manipulator link	m_l	0.065	Kg

2.1. Forward Kinematics

The forward kinematics computes the cartesian coordinates of Quanser 2-DOF robot end effector based on the actuated angles θ_A and θ_B of servos A and B respectively. The 2-DOF manipulator consists of a four bar linkage structure having equal length, denoted by L_b . The forward kinematics of the robotic manipulator is shown in Fig. 2, where the end effector's position is denoted by joint E.

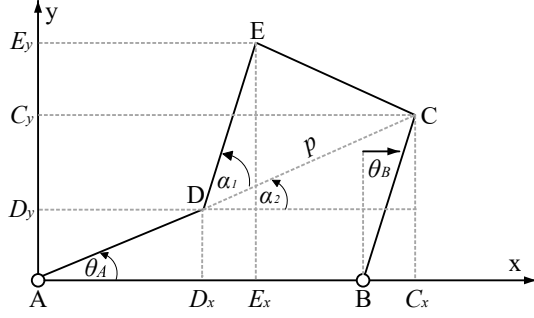


Fig. 2. Forward kinematics of pantograph robot.

Looking at the top of the manipulator, the anticlockwise rotation of the actuator's angles is taken as positive. The cartesian coordinates of joints D and C are given by

$$\begin{aligned} D_x &= L_b \cos(\theta_A) & D_y &= L_b \sin(\theta_A) \\ C_x &= B - L_b \sin(\theta_B) & C_y &= L_b \cos(\theta_B) \end{aligned}$$

Referring to Fig. 2, the distance between point D and C can be computed by applying Pythagoras theorem. The triangle CDE is an isosceles and all its sides are known. So, the angles α_1 and α_2 at vertex D can be expressed as

$$\alpha_1 = \arccos \frac{p}{2L_b} \quad (3)$$

$$\alpha_2 = \arctan \frac{C_y - D_y}{C_x - D_x} \quad (4)$$

Using trigonometry, forward kinematics of end effector's position can be written as,

$$E_x = D_x + L_b \cos(\alpha_1 + \alpha_2) \quad (5)$$

$$E_y = D_y + L_b \sin(\alpha_1 + \alpha_2) \quad (6)$$

2.2. Inverse Kinematics

The inverse kinematics (IK) finds the actuated angles of two SRV02 plants from the cartesian coordinates of the end effector of the manipulator. The known quantities in IK are E_x and E_y coordinates of the location E, as illustrated in Fig. 3.

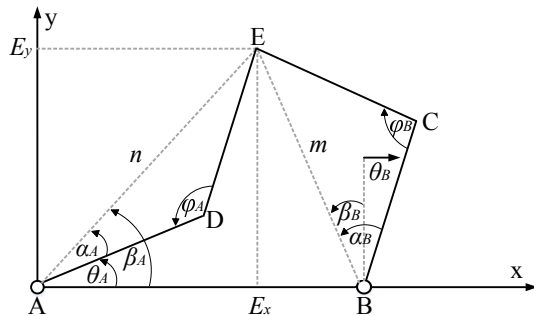


Fig. 3. Inverse kinematics of pantograph robot.

Considering triangle $\triangle ABE$, the sides represented by m and n can be expressed in terms of position of the end effector as

$$n = \sqrt{E_x^2 + E_y^2} \quad (7)$$

$$m = \sqrt{(B - E_x)^2 + E_y^2} \quad (8)$$

Using trigonometry, the angles ϕ_A and ϕ_B can be given by

$$\phi_A = \arccos\left(1 - \frac{n^2}{2L_b^2}\right) \quad (9)$$

$$\phi_B = \arccos\left(1 - \frac{m^2}{2L_b^2}\right) \quad (10)$$

By using angles sum theorem for triangles and solving for

$$\alpha_A = \frac{\pi - \phi_A}{2} \quad (11)$$

$$\alpha_B = \frac{\pi - \phi_B}{2} \quad (12)$$

$$\beta_A = \arctan(E_y/E_x) \quad (13)$$

$$\beta_B = \arctan\left(\frac{B - E_x}{E_y}\right) \quad (14)$$

Finally, the servo actuators angles can be calculated as

$$\theta_A = \beta_A - \alpha_A \quad (15)$$

$$\theta_B = \beta_B - \alpha_B \quad (16)$$

3. CONTROL STRATEGIES

The theoretical background of conventional PID, LQR and FCPC control schemes are discussed as follows:

3.1. PID controller

Among the linear control strategies, PID is a simple model-free control technique and is commonly used because of its simplicity [27]. The control algorithm comprises of three modes, i.e., proportional, differential, and integral. In this research, PID control is designed and is implemented on hardware (see section 6) to validate its performance for the position control of the SRV02 system. The control law is given by (17)

$$u_{pid} = k_p \theta_e + k_d \dot{\theta}_e + k_i \int \theta_e dt \quad (17)$$

where k_p , k_d and k_i are PID tuning gains and (θ_e) is the position tracking error between measured angle θ and the desire angle (θ_d) of SRV02 link. Designing a PID controller appears to be conceptually intuitive since the designed gains are repeatedly adjusted and are then incorporated into real-time Simulink model to achieve the desired performance.

3.2. Linear quadratic regulator

Among the modern optimal control techniques, LQR is widely used [28]. The control algorithm uses the dynamic model with complete information of the system to minimize quadratic performance index given by (18) and calculates the optimal gains to enhance the system performance.

$$J(x, t) = \int_0^{\infty} (x^T Q x + u^T R u) dt \quad (18)$$

The weight matrices Q and R are tuning variables and penalize states x and control input u respectively. The feedback control law can be designed as

$$u_{lqr} = -kx \quad (19)$$

where k denotes optimal feedback gains and is given by

$$k = R^{-1} B^T P \quad (20)$$

where $P = P^T \geq 0$ is a solution of algebraic Riccati equation i.e.

$$A^T P + PA - PBR^{-1}B^T P = 0 \quad (21)$$

3.3. Collaborative position controller

The fixed-weighted collaborative position controller (FCPC) synthesizes a synergistic control scheme utilizing the designed PID and LQR controllers [14–16]. To overcome the drawbacks of each controller and to utilize their benefits, both the controllers are linearly augmented. Block diagram of the proposed control scheme is shown in Fig. 4. The associated control law in continuous time can be defined as,

$$u = hu_{pid} + (1 - h)u_{lqr} \quad (22)$$

where $h \in [0, 1]$ characterizes weights of PID and LQR. The weightage parameter in FCPC is tuned using PSO explained in section 4.

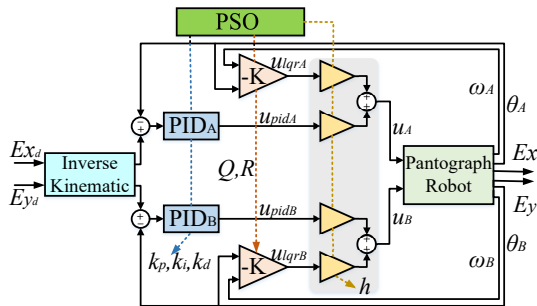


Fig. 4. Fixed-weighted collaborative position controller.

4. PARTICLE SWARM OPTIMIZATION

The PSO algorithm is a population-based optimization technique [29]. A population of random particles is initially selected for optimal tuning of the gains/parameters. It then searches the entire space to converge to the global best-fit solution. Each particle has a position (X_i) and velocity (V_i) associated with it. The relationship used to update the position and velocity of a particle are given as

$$X_i = X_i + V_i \quad (23)$$

$$V_i = w_i V_i + m_1 r_1 (P_i - X_i) + m_2 r_2 (P_g - X_i) \quad (24)$$

where m_1 and m_2 are cognitive coefficients, r_1 and r_2 are random real numbers and w is the inertia weight. The first term of (24) denotes the current motion of a particle, while the second term is called as ‘cognitive term’ which is the difference between current position of a particle and its best local position (P_i). The third term is known as ‘social term’ which is the difference between current position of a particle and global best swarm position (P_g). In this work, the PID gains, LQR weighting matrices, and weightage parameter in FCPC are optimally tuned. After initialization, the PSO algorithm iteratively computes and stores the fitness values of each particle using (25)

$$Fitness = OS^2 + T_s^2 + \int (0.001\theta_e^2 + 0.05v_m^2) dt \quad (25)$$

where OS denotes overshoot, T_s is settling time, θ_e is position tracking error and v_m is the applied voltage. The optimization problem is to minimize the fitness function (25) to ensure less overshoot and fast response of the system. The integral-squared-error (ISE) and integral-squared input voltage performance indices are used to achieve the optimal control effort. For each particle, the fitness value is compared with the existing best objective value also called as ‘local best’ (P_i). The particle with highest fitness value is updated as new P_i and is chosen as ‘global best’ (P_g) [30]. The optimizer inertia weight (ω_j) given in (26) decreases from 1 to 0 in each iteration in order to explore the best solution in search space.

$$\omega_j = \omega_{max} \left(\frac{\omega_{max} - \omega_{min}}{j_{max}} \right) j \quad (26)$$

where j and j_{max} are current iteration and maximum defined iteration respectively, ω_{max} and ω_{min} are set at 0.902 and 0.394 respectively. The flowchart of the PSO algorithm is shown in Fig. 5. A population of 100 particle candidates is taken for optimization of the fitness function. For the PID and LQR schemes, each particle has a set of three members $X_i = [k_p, k_i, k_d]$ and $X_i = [q_{11}, q_{22}, r]$ respectively. It means that the particles fly in a three-dimensional space and searches for the optimal values of the gains. For the proposed FCPC, each particle has one member h and moves along a line. During each iteration, as the particles

assume new positions X_i , the gains values are used to run the 2DOF and the fitness is evaluated according to (25). The local best of each particle is saved as P_i , and the particle with minimum fitness value is added as the global best variable P_g . To optimally tune the control laws and to minimize the fitness function, 20 iterations have been performed as shown in Fig. 6. It can be seen that the PID controller takes less iterations to reach its optimum solution as compared to the LQR and FCPC schemes. Conversely, the optimization process of the FCPC results in smaller fitness value. Therefore, PSO-FCPC is the best option to control 2-DOF end effector. The average elapsed time is recorded as $T_a = \sum_{i=1}^{j_{max}} \frac{T(j)}{j}$, where $T(j)$ is the elapsed time for each iteration. The average time is same for tuning the inputs (17), (19) and (22) and is given as $T_a = 9.02$ sec. The optimized gain values of the proposed control schemes, their ranges, and the corresponding values of the fitness function are presented in Table 2.

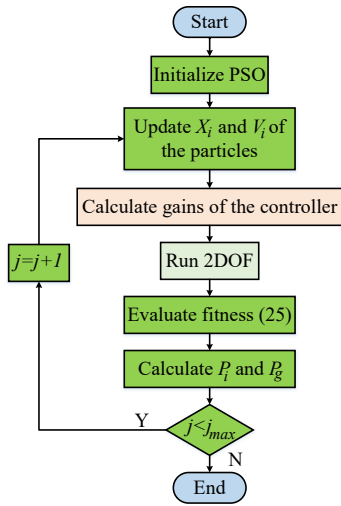


Fig. 5. Flowchart of the optimization process.

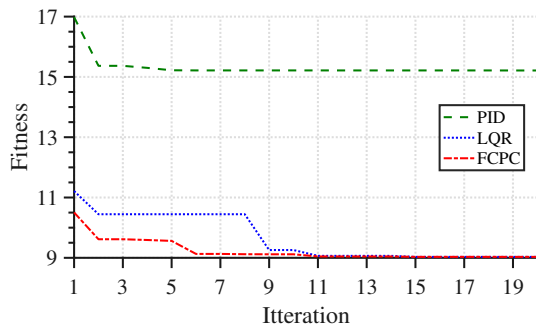


Fig. 6. Evolving process of the fitness function value for the proposed controllers using PSO.

Table 2. Optimized parameters values for the proposed control schemes.

Gain	Control Scheme						
	PID			LQR			FCPC
Value	k_p	k_i	k_d	q_{11}	q_{22}	r	h
Value	0.05	0.015	0.004	0.14	0.107	0.11	0.43
Range	[0, 1]	[0, 1]	[0, 0.5]	[0, 1]	[0, 1]	[0, 1]	[0, 1]
Fitness	15.21	19.12	16.12	10.04	9.03	9.03	9.031

5. EXPERIMENTAL SETUP

The experimental test bench centered on Quanser 2-DOF robotic manipulator is presented in Fig. 7.

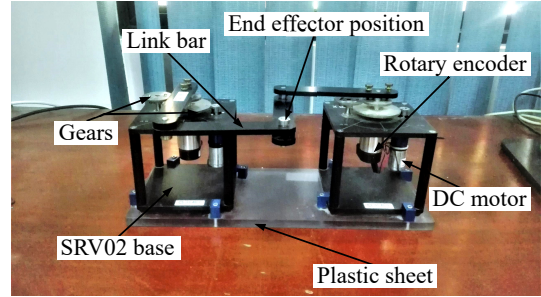


Fig. 7. Quanser 2-DOF pantograph robot at home position.

The hardware setup consists of two SRV02 plants connected together via four link bars having same lengths and a Q3 Control PaQ-FW data acquisition device interfaced with MATLAB/Simulink running on a PC as shown in Fig. 8.

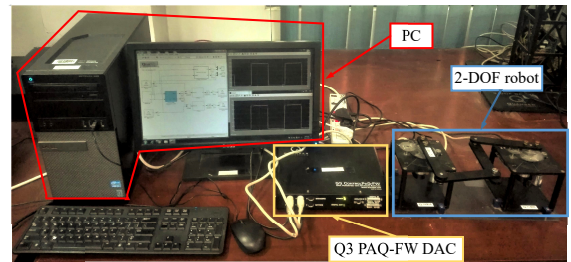


Fig. 8. Experimental setup of 2-DOF pantograph robot.

The whole setup is implemented via hardware in loop (HIL) experiments. SRV02 comprises of a DC motor with planetary gearbox, motor pinion gears, load gears, potentiometer backlash gears and ball bearing block. The plant comes with a built-in potentiometer and a high-resolution encoder providing 4096 counts per revolution to measure the position of the load link. The Q3 control PaQ-FW is an advanced HIL control board that can be easily interfaced with MATLAB or LABVIEW with an available 6-pin FireWire (IEEE 1394) input to perform a wide range of

laboratory experiments. The control board comes with a built-in power amplifier and a data acquisition card. It supports 16-bit three encoder input channels numbered from 0-2. The two encoder channels, i.e., channels 0 and 1 are configured in HIL initialized block to read angular position data of both SRV02 plants. In addition, three PWM outputs channels are available in which two of them are used to drive the SRV02 motors.

6. TESTS AND RESULTS

To characterize the performance of the proposed control laws, real-time tests have been performed using the QUARC library installed in MATLAB 2009a, running on a computer system with the following specifications; Dell OptiPlex 990, Intel(R) Core(TM) i3-2120 CPU @ 3.30GHz, 32-bit Operating System. The resulting responses are graphically visualized and recorded for two different cases.

Case 1: In this case, the experiment is conducted to investigate the tracking performance of the manipulator's end effector for a square reference signal using the designed control laws. The control parameters are taken from Table 2. The end effector of the robotic manipulator is initially set at home position i.e., $(E_{x0}, E_{y0}) = (L_b, L_b)$ assuming the joint angles are at the origin. A square wave signal is applied as a position reference trajectory.

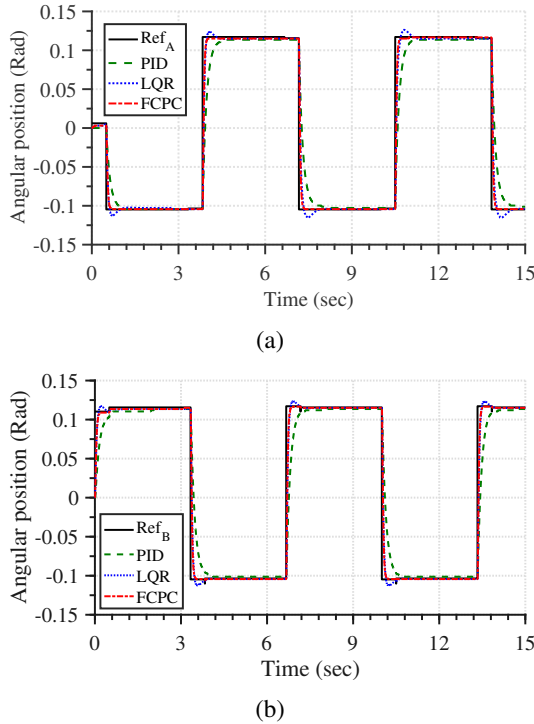


Fig. 9. Angular position responses of (a) actuator A (b) actuator B.

Fig. 9 show experimental results of the proposed optimal control laws in which the position tracking performance of SRV02 actuators is presented. The results demonstrate that using FCPC approach, the actuator load shaft tracks the desired position with a reasonable steady-state as well as transient performance. Based on the derived forward kinematics, the position of the manipulator's end effector on the x-axis and y-axis is depicted in Fig. 10a and Fig. 10b respectively. It is clear that the PID controller gives poor transient performance. The LQR controller exhibits good transient behavior but with poor steady-state response due to lack of integral action. As evident from the results, the performance with FCPC is superior than with PID controller in terms of transient response, while the achieved steady-state response with FCPS is better than obtained with LQR control scheme.

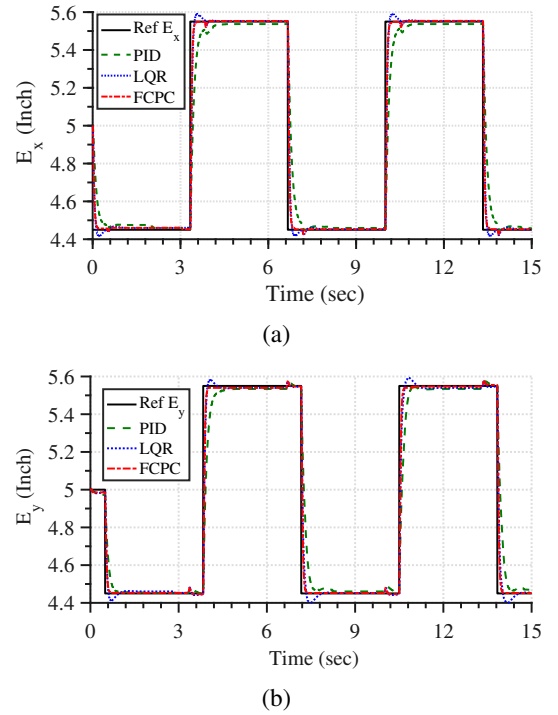


Fig. 10. Trajectory tracking of manipulator's end effector along (a) x-axis (b) y-axis.

Fig. 11 demonstrates the two-dimensional path drawn by the manipulator's end effector. It can be observed that LQR exhibits relatively fast response with an overshoot of 2.025%. FCPC scheme surpasses the PID and LQR responses. For each of the three control schemes, experimental test results are given in Table 3. The hardware results clearly manifest that the PSO based FSPC control strategy is superior in tracking than other two optimal control schemes.

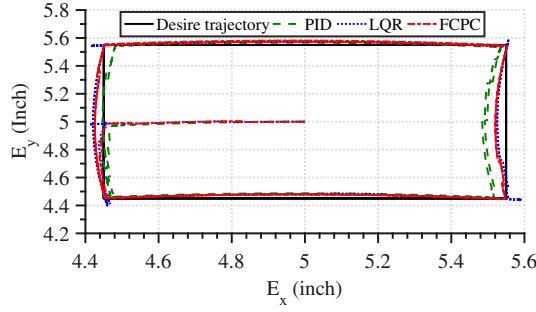


Fig. 11. Manipulator tracking performance in Cartesian plane.

Case 2: In this case, we considered the desired end-effector position as $E_{x_d} = L_b + 0.5 \sin(\omega t)$ with $\omega = 0.471$. The y-component is chosen as $E_{y_d} = 0$ for $t < 0.5$ sec and $E_{y_d} = L_b + 0.5 \sin(\omega t - 0.5)$ for $t \geq 0.5$ sec as shown in Fig. 13. The manipulator is set to the same initial position as that of case 1. The actuator's tracking performance is illustrated in Fig. 12. From the rotary servos data, the manipulator's positions are calculated using (5) and (6) and are plotted in Fig. 13. Fig. 14 depicts the tracking performance given by the three control schemes in xy plane. The FCPC scheme proposed in (22) provides more optimal tracking performance as shown in the zoomed view of Fig. 14.

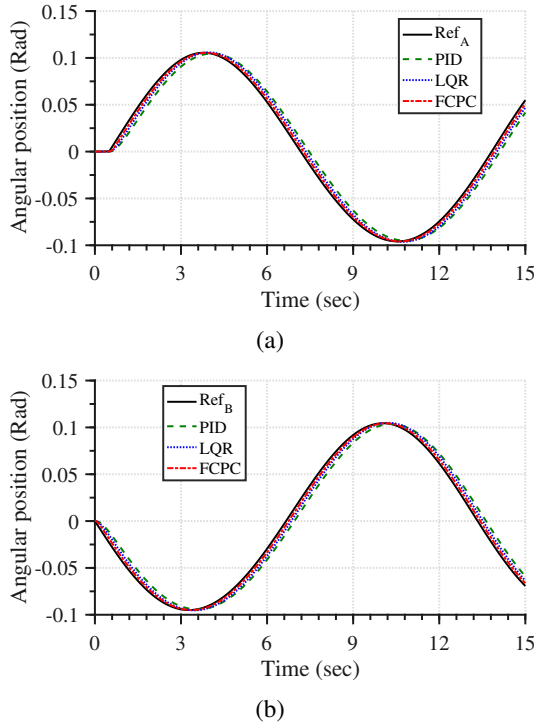
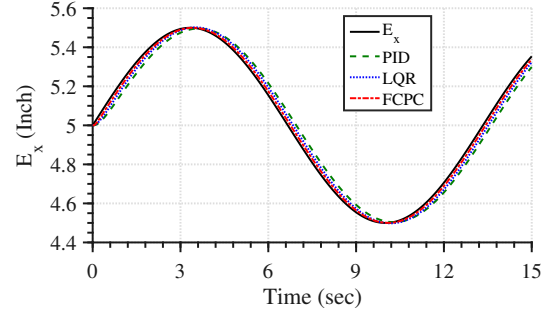


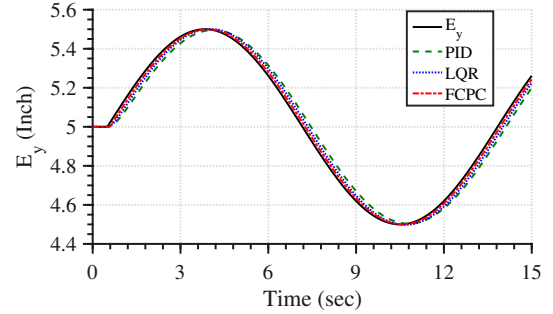
Fig. 12. Angular position responses of (a) actuator A (b) actuator B.

Table 3. Performance comparison of the proposed control laws.

Controller	Performance			
	T_r (sec)	T_s (sec)	e_{ss} (Inch)	%OS
PID	0.28	0.79	0.01	0
LQR	0.09	0.212	0.01	2.025
FCPC	0.092	0.231	0.009	0



(a)



(b)

Fig. 13. Sinusoidal trajectory tracking of manipulator's end effector along (a) x-axis (b) y-axis.

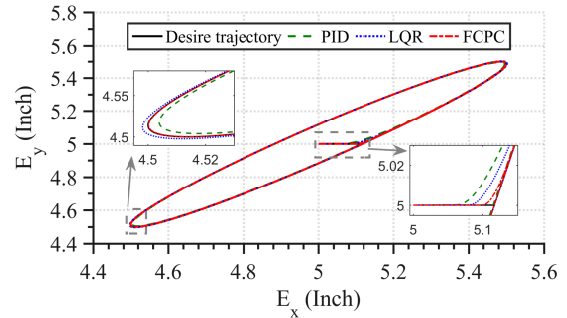


Fig. 14. Desired trajectory tracking results of manipulator's end effector in xy plane.

To analyze the results in case 1 and case 2, the performance index Integral Time Absolute Error (ITAE) i.e.,

$ITAE = \int t|e_i|dt$ values for $i = x; y$ are calculated to characterize the tracking performance. Based on the results in Fig. 15, it can be concluded that the optimally tuned FCPC in (22) demonstrates superior tracking performance in comparison to the optimal PID and LQR counterparts expressed in (17) and (19), respectively.

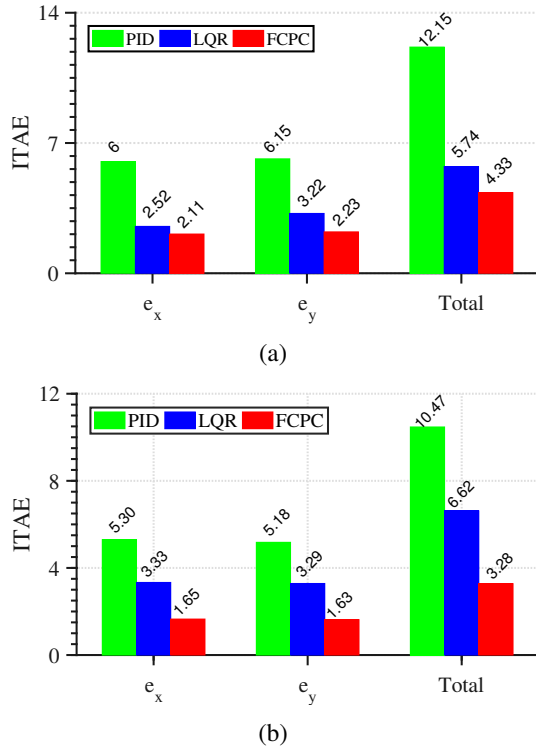


Fig. 15. Performance comparison for (a) case 1 (b) case 2.

7. CONCLUSION

This research models Quanser 2-DOF robotic manipulator and addresses its behavior including the actuator dynamics to design optimal control approaches. Modeling of the robot involves derivation of dynamics of rotary actuators and manipulator kinematics. The optimal control techniques under study include PID, LQR and FCPC. The experimental validation of proposed control techniques has been carried out on a robotic manipulator consisting of four bar linkages and two rotary servo plants. PID approach resulted poor transient performance, the LQR overcomes the shortcoming of PID but demonstrates unwanted overshoots. The proposed FCPC scheme synthesizes a control law that collaborates the individual control efforts provided independently by PID and LQR. The actual position quickly converges to the desired trajectory demonstrating 10% improvement in steady-state error and about 37% in transient response as compared to the individual efforts of PID and LQR. In future, the optimal weighted combination of model-based nonlinear con-

trol schemes can be tested to control the manipulator end effector position using hybrid PSO and Grey Wolf Optimizer. Also, it is anticipated in near future to evaluate the performance improvement in the presence of disturbances.

REFERENCES

- [1] J. Iqbal, R. U. Islam, S. Z. Abbas, A. A. Khan, and S. A. Ajwad, "Automating industrial tasks through mechatronic systems a review of robotics in industrial perspective," *Tehnički vjesnik*, vol. 23, no. 3, pp. 917-924, 2016.
- [2] R. Samah, M. Kidouche, and A. Rezoug, "Adaptive robust nonsingular terminal sliding mode design controller for quadrotor aerial manipulator," *Telkomnika*, vol. 17, no. 3, pp. 1501-1512, 2019.
- [3] J. Seo, J. Kim, S. Park, and J. Cho, "A SLIP-based robot leg for decoupled spring-like behavior: Design and evaluation," *International Journal of Control, Automation and Systems*, vol. 17, no. 9, pp. 2388-2399, 2019.
- [4] J. Iqbal, M. Ullah, S. G. Khan, B. Khelifa, and S. Ćuković, "Nonlinear control systems- A brief overview of historical and recent advances," *Nonlinear Engineering*, vol. 6, no. 4, pp. 301-312, 2017.
- [5] J. Iqbal, "Modern Control Laws for an Articulated Robotic Arm: Modeling and simulation," *Engineering, Technology & Applied Science Research*, vol. 9, no. 2 pp. 4057-4061, 2019.
- [6] Z. S. Awan, K. Ali, J. Iqbal, and A. Mehmood, "Adaptive backstepping based sensor and actuator fault tolerant control of a manipulator," *Journal of Electrical Engineering and Technology*, vol. 14, no. 2, pp. 2497-2504, 2019.
- [7] W. Alam, S. Ahmad, A. Mehmood, and J. Iqbal, "Robust sliding mode control for flexible joint robotic manipulator via disturbance observer," *Description of Complex Systems: INDECS*, vol. 17, no. 1-B, pp. 85-97, 2019.
- [8] O. Khan, M. Pervaiz, E. Ahmad, and J. Iqbal, "On the derivation of novel model and sophisticated control of flexible joint manipulator," *Revue Roumaine des Sciences Techniques-Serie Electrotechnique et Energetique*, vol. 62, no. 1, pp. 103-108, 2017.
- [9] S. Khan, S. Bendoukha, W. Naeem, and J. Iqbal, "Experimental validation of an integral sliding mode-based LQG for the pitch control of a UAV-mimicking platform," *Advances in Electrical and Electronics Engineering*, vol. 17, no. 3, pp. 275-284, 2019.
- [10] N. Ali, W. Alam, A. Ur Rehman, and M. Pervaiz, "State and Disturbance Observer Based Control for a Class of Linear Uncertain Systems," *Proc. of the International Conf. on Frontiers of Information Technology*, pp. 139-143, 2017.
- [11] S. A. Ajwad, J. Iqbal, R. U. Islam, A. Alsheikhy, A. Almeshal, and A. Mehmood, "Optimal and robust control of multi DOF robotic manipulator: Design and hardware realization," *Cybernetics and Systems*, vol. 49, no.1, pp. 77-93, 2018.

- [12] H. Feng, C. B. Yin, W. W. Weng, W. Ma, J. J. Zhou, W. H. Jia and Z. L. Zhang, "Robotic excavator trajectory control using an improved GA based PID controller," *Mechanical Systems and Signal Processing*, vol. 105, pp. 153-168, 2018.
- [13] H. V. H. Ayala, and L. dos Santos Coelho, "Tuning of PID controller based on a multiobjective genetic algorithm applied to a robotic manipulator," *Expert Systems with Applications*, vol. 39, no. 10, pp. 8968-8974, 2012.
- [14] L. Sun, and J. Gan, "Researching of two-wheeled self-balancing robot base on LQR combined with PID" *Proc. of the 2nd International Workshop on Intelligent Systems and Applications*, pp. 1-5, 2010.
- [15] S. Bagheri, T. Jafarov, L. Freidovich, and N. Sepehri, "Beneficially combining LQR and PID to control longitudinal dynamics of a SmartFly UAV," *Proc. of the 7th Annual Information Technology, Electronics and Mobile Communication Conference*, pp. 1-6, 2016.
- [16] R. M. Asl, A. Mahdoudi, E. Pourabdollah, and G. Klančar, "Combined PID and LQR controller using optimized fuzzy rules," *Soft Computing*, vol. 23, no. 13, pp. 5143-5155, 2019.
- [17] G. Ghosh, P. Mandal, and S. C. Mondal, "Modeling and optimization of surface roughness in keyway milling using ANN, genetic algorithm, and particle swarm optimization," *The International Journal of Advanced Manufacturing Technology*, vol. 100, no. 5, pp. 1223-1242, 2019.
- [18] G. I. Sayed, A. Tharwat, and A. E. Hassanien, "Chaotic dragonfly algorithm: an improved metaheuristic algorithm for feature selection," *Applied Intelligence*, vol. 49, no. 1, pp. 188-205, 2019.
- [19] D. Fister, I. Fister Jr, I. Fister and R. Šafarič, "Parameter tuning of PID controller with reactive nature-inspired algorithms," *Robotics and Autonomous Systems*, vol. 84, pp. 64-75, 2016.
- [20] A. Al-Mahturi, and H. Wahid, "Optimal tuning of linear quadratic regulator controller using a particle swarm optimization for two-rotor aerodynamical system," *International Journal of Electronics and Communication Engineering*, vol. 11, no. 2, pp. 184-190, 2017.
- [21] V. Saisudha, G. Seeja, R. Pillay, G. Manikutty, and R. Bhavani, "Analysis of speed control of DC motor using LQR method," *International Journal of Control Theory and Applications*, vol. 9, no.15, pp. 7377-7385, 2016.
- [22] H. Freire, and P. B. Moura Oliveira, and E. J. Solteiro Pires, "From single to many-objective PID controller design using particle swarm optimization," *International Journal of Control, Automation and Systems*, vol. 15, no. 2, pp. 918-932, 2017.
- [23] J. Y. Jhang, C. J. Lin, C. T. Lin, and K. Y. Young, "Navigation control of mobile robots using an interval type-2 fuzzy controller based on dynamic-group particle swarm optimization," *International Journal of Control, Automation and Systems*, vol. 16, no. 5, pp. 2446-2457, 2018.
- [24] *Quanser handout, Rotary Servo Base Unit*, accessed on October 31, 2019. Available on: <https://www.quanser.com/products/rotary-servo-base-unit/>
- [25] I. M. Mehedi, U. Ansari, U. M. Al-Saggaf, and A. H. Bajodah, "Controlling a rotary servo cart system using robust generalized dynamic inversion," *International Journal of Robotics and Automation*, vol. 35, no. 1, pp. 77-85, 2020.
- [26] K. Latha, V. Rajinikanth, and P. M. Surekha, "PSO-Based PID Controller Design for a Class of Stable and Unstable Systems," *ISRN Artificial Intelligence*, vol. 2013, 2013. <https://doi.org/10.1155/2013/543607>
- [27] M. Wasim, M. Ullah, and J. Iqbal, "Gain-scheduled proportional integral derivative control of taxi model of unmanned aerial vehicles," *Revue Roumaine des Sciences Techniques-Serie Electrotechnique et Energetique*, vol. 64, no. 1, pp. 75-80, 2019.
- [28] O. Saleem, and M. Rizwan, "Performance optimization of LQR-based PID controller for DC-DC buck converter via iterative-learning-tuning of state-weighting matrix," *International Journal of Numerical Modelling: Electronic Networks, Devices and Fields*, vol. 32, no. 3, pp. e2572, 2019.
- [29] Z. Bingül, and O. Karahan, "A Fuzzy Logic Controller tuned with PSO for 2DOF robot trajectory control," *Expert Systems with Applications*, vol.38, no.1, pp.1017-1031, 2011.
- [30] A. R. Bhatti, Z. Salam, B. Sultana, N. Rasheed, A. B. Awan, U. Sultana and M. Younas, "Optimized sizing of photovoltaic grid-connected electric vehicle charging system using particle swarm optimization," *International Journal of Energy Research*, vol. 43, no. 1, pp. 500-522, 2019.